

Flood Risks in Sinking Delta Cities: Time for a Reevaluation?

Yin, Jie; Jonkman, Sebastiaan; Lin, Ning; Yu, Dapeng; Aerts, Jeroen; Wilby, Robert; Pan, Ming; Bricker, Jeremy; Ke, Qian; More Authors

DOI

[10.1029/2020EF001614](https://doi.org/10.1029/2020EF001614)

Publication date

2020

Document Version

Final published version

Published in

Earth's Future

Citation (APA)

Yin, J., Jonkman, S., Lin, N., Yu, D., Aerts, J., Wilby, R., Pan, M., Bricker, J., Ke, Q., & More Authors (2020). Flood Risks in Sinking Delta Cities: Time for a Reevaluation? *Earth's Future*, 8(8), 1-15. Article e2020EF001614. <https://doi.org/10.1029/2020EF001614>

Important note

To cite this publication, please use the final published version (if applicable). Please check the document version above.

Copyright

Other than for strictly personal use, it is not permitted to download, forward or distribute the text or part of it, without the consent of the author(s) and/or copyright holder(s), unless the work is under an open content license such as Creative Commons.

Takedown policy

Please contact us and provide details if you believe this document breaches copyrights. We will remove access to the work immediately and investigate your claim.

Flood Risks in Sinking Delta Cities: Time for a Reevaluation?

Key Points:

- We combine reliability analysis with hydrodynamic modeling to quantify relative SLR effect on dike failures and flood hazards for Shanghai
- Relative SLR may result in unprecedented and nonlinear impacts on dike failure-induced flooding in Shanghai and other sinking delta cities
- Including reliability-based dike failures in flood simulations contributes to more robust flood risk assessment for sinking delta cities

Supporting Information:

- Supporting Information S1

Correspondence to:

J. Yin and D. Yu,
jyin@geo.ecnu.edu.cn;
d.yu2@lboro.ac.uk

Citation:

Yin, J., Jonkman, S., Lin, N., Yu, D., Aerts, J., Wilby, R., et al. (2020). Flood risks in sinking delta cities: Time for a reevaluation?. *Earth's Future*, 8, e2020EF001614. <https://doi.org/10.1029/2020EF001614>

Received 6 MAY 2020

Accepted 22 JUL 2020

Accepted article online 3 AUG 2020

Author Contributions:

Conceptualization: Jie Yin, Jeroen Aerts

Data curation: Jun Wang

Formal analysis: Jie Yin

Investigation: Jie Yin

Methodology: Jie Yin, Sebastiaan Jonkman, Dapeng Yu, Jeremy Bricker, Qian Ke, Qing Zhao, Jianzhong Ge

Project administration: Jie Yin

Resources: Jie Yin

Visualization: Jie Yin

Writing - original draft: Jie Yin

Writing - review & editing: Jie Yin, Sebastiaan Jonkman, Ning Lin, Dapeng (continued)

©2020. The Authors.

This is an open access article under the terms of the Creative Commons Attribution-NonCommercial-NoDerivs License, which permits use and distribution in any medium, provided the original work is properly cited, the use is non-commercial and no modifications or adaptations are made.

Jie Yin^{1,2,3} , Sebastiaan Jonkman⁴ , Ning Lin³ , Dapeng Yu⁵ , Jeroen Aerts⁶, Robert Wilby⁵ , Ming Pan³ , Eric Wood³ , Jeremy Bricker⁴, Qian Ke⁴, Zhenzhong Zeng^{3,7} , Qing Zhao¹, Jianzhong Ge⁸ , and Jun Wang¹

¹Key Laboratory of Geographic Information Science (Ministry of Education), East China Normal University, Shanghai, China, ²Institute of Eco-Chongming, East China Normal University, Shanghai, China, ³Department of Civil and Environmental Engineering, Princeton University, Princeton, NJ, USA, ⁴Department of Hydraulic Engineering, Delft University of Technology, Delft, The Netherlands, ⁵Geography and Environment, Loughborough University, Loughborough, UK, ⁶The Institute for Environmental Studies, Vrije Universiteit Amsterdam, Amsterdam, The Netherlands, ⁷School of Environmental Science and Engineering, Southern University of Science and Technology, Shenzhen, China, ⁸State Key Laboratory of Estuarine and Coastal Research, East China Normal University, Shanghai, China

Abstract Sea level rise (SLR) and subsidence are expected to increase the risk of flooding and reliance on flood defenses for cities built on deltas. Here, we combine reliability analysis with hydrodynamic modeling to quantify the effect of projected relative SLR on dike failures and flood hazards for Shanghai, one of the most exposed delta cities. We find that flood inundation is likely to occur in low-lying and poorly protected periurban/rural areas of the city even under the present-day sea level. However, without adaptation measures, the risk increases by a factor of 3–160 across the densely populated floodplain under projected SLR to 2100. Impacts of frequent flood events are predicted to be more affected by SLR than those with longer return periods. Our results imply that including reliability-based dike failures in flood simulations enables more credible flood risk assessment for global delta cities where conventional methods have assumed either overtopping only or complete failure.

Plain Language Summary Sea level rise is expected to exacerbate dike failures and flood hazards in sinking delta cities. With the case in Shanghai, we demonstrate that flood risks in many delta cities globally could be better understood, as most flood risk modeling exercises assumed either complete dike failure or overtopping only but neglected the interaction between dike reliability, land subsidence, and flood risks, thereby likely either overestimating or underestimating future risks. The transferrable framework presented herein contributes to more robust risk assessments for other global delta cities facing significant relative sea level rise and flooding challenges.

1. Introduction

Flooding is among the most common and devastating natural hazards, accounting for approximately one third of all global disaster losses and over half of total casualties (Douben, 2006). The containment of floods has evolved with the development of human settlement since 7,000 years ago, especially in low-lying delta areas (Giosan et al., 2014; Nienhuis et al., 2020; Tessler et al., 2015). Delta cities are high-density agglomerations of population and assets that are particularly susceptible to flooding from various sources (i.e., pluvial, fluvial, coastal, and groundwater). Over recent decades, storm-induced flood catastrophes appear to be happening more frequently and are raising concern among vulnerable populations in major, flood-prone delta cities. For example, flooding of New Orleans due to Hurricane Katrina (2005) caused 1,833 fatalities and more than \$125 billion in losses, making it the costliest cyclone in history (Kates et al., 2006). A more recent calamity was associated with Typhoon Hato in 2017, which led to almost one third of Macau (on the Pearl River Delta) to be heavily flooded with 10 deaths, 244 injuries, and \$7.8 billion damages. Flood exposures and risks in delta cities are projected to increase in a changing environment, if no actions are taken (Hallegatte et al., 2013; Hanson et al., 2011; Jongman et al., 2012; Winsemius et al., 2016).

Climate change in combination with rapid urbanization are key drivers of an intensified hydrologic regime and enhanced flood risk (Hinkel et al., 2014; IPCC, 2013, 2014; Zhang et al., 2018). Sea level rise (SLR)

Yu,
Jeroen Aerts, Robert Wilby, Ming Pan,
Eric Wood, Jeremy Bricker, Qian Ke,
Zhenzhong Zeng, Qing Zhao,
Jianzhong Ge

amplifies coastal flood hazards by raising baseline water levels for a tidal wave to build upon (Arns et al., 2017; Li et al., 2018; Woodruff et al., 2013). Moreover, nonclimatic local processes, such as land subsidence caused by tectonics, natural sediment compaction, and aquifer dewatering, play another important role in exacerbating flood risk in deltaic zones by contributing to the rate of relative SLR (Brown & Nicholls, 2015; Dixon et al., 2006; Ericson et al., 2006; Miller et al., 2013; Minderhoud et al., 2019; Törnqvist et al., 2008). According to remotely sensed geodetic measurements, the majority of the world's large deltas are sinking more rapidly than geocentric sea level is rising, due to reduced aggradation and/or accelerated compaction (Shirzaei & Bürgmann, 2018; Syvitski et al., 2009). Upstream trapping of sediments by dams reduces the volume deposited on deltas, which in turn slows the growth of the deltas and accelerates coastal erosion (Hoitink et al., 2020; Nienhuis et al., 2018). Expanding human footprints on deltas through residential occupation and coastal development further increases exposure to flooding. The net effect of these processes is evident in New Orleans and Shanghai, where levels have subsided by more than 3 m since the middle to late nineteenth century, mainly due to excessive groundwater extraction and large-scale construction (Dixon, 2008; Gong & Yang, 2008).

In response, human society has been seeking to defend delta plains from flooding for a long time (Dawson et al., 2011). Physical engineering measures, such as barriers and dikes, are often seen as a cost-effective way of protecting densely populated deltaic settlements (Jongman, 2018; Ward et al., 2017). Wealthier delta cities that experience frequent flood hazards are usually better protected to higher standards (Xian et al., 2018). For instance, major cities in Dutch Delta are protected with a series of dikes and storm surge barriers (the "Delta Works") to a standard of the 1 in 10,000-year flood event. Such measures have proved to be successful but depend on a high level of routine maintenance (Yin et al., 2015). While providing protection against low probability floods, artificial dikes may fail due to a combination of high water loading, wave attack, and/or long flood duration (Vorogushyn et al., 2010). Dike failure can also occur as a result of long-term structure deformation, the magnitude of which can be much greater than hinterland subsidence in delta cities, such as New Orleans and Shanghai (Dixon et al., 2006; Yin et al., 2019). Among various failure mechanisms, dike breach or flow over the crest of dikes are the two major modes causing significant hinterland inundation and damages. Hence, it is crucial to understand the functional failures of flood protection structures and the resultant flood potentials in deltaic flood risk management.

Considerable progresses have been made in the assessment of dike reliability and flood hazards. Various limit state equations can be used to analyze specific failure mechanisms (e.g., overtopping, breaching, piping, erosion, and slope instability) in coastal and/or fluvial dike systems (Curran et al., 2018; Naulin et al., 2015). The probability of dike failure can be described in a "reliability analysis" as a function of hydraulic loading variables (e.g., water level and/or duration) by 1-D fragility curves and/or 2-D fragility surfaces (Apel et al., 2004; Dawson et al., 2005; Hall et al., 2003; Vorogushyn et al., 2009). More recently, reliability analysis has been coupled with 1-D and/or 2-D hydraulic models for the purpose of inundation mapping and flood hazard assessment. For example, the Inundation Hazard Assessment Model, which comprises an unsteady 1-D hydrodynamic model for river channel routing, a probabilistic dike breach model for reliability analysis, and a 2-D raster-based inundation model, was developed for the simulation of floodplain flow in the case of dike failures (Vorogushyn et al., 2010). Nevertheless, there are two main limitations to the existing studies. First, SLR and land subsidence (including structure deformation) have not been adequately considered when quantifying dike failure-induced flood hazards for delta cities. Second, a simplifying assumption is often made that the protection standard equals the probability of flooding, which does not consider the actual state of the defenses, hence introducing uncertainties and bias in the modeled flood inundation patterns (Jonkman, 2013).

To address these research gaps, an interdisciplinary process-based approach is developed for more robust estimation of dike reliability and associated flood hazards under the effect of relative SLR (both SLR and vertical land movements) for deltaic cities. The hybrid methodology is applied to the metropolitan region of Shanghai, which is one of the most exposed delta cities to flooding globally and hence completely relies on protection from the dike system. Specifically, interferometric synthetic aperture radar (InSAR) measurements are utilized to obtain detailed subsidence rates of the coastal dike system. We combine state-of-the-art projections of relative SLR and advanced structural failure models to explicitly determine potential flood defense overtopping and/or breach locations along the coast and river. We then apply a fine-resolution hydrodynamic model to derive evolving flood inundation caused by the compound effects of dike breach

and overtopping by the end of the 21st century. As far as we are aware, this is the first attempt to comprehensively assess the combined impacts of long term SLR and land subsidence on dike failures and resultant flood hazards for large-scale delta cities protected by flood defenses. With the case study in Shanghai, we demonstrate that flood risks in many delta cities globally could be better understood, as most flood risk modeling exercises assumed either complete dike failure or overtopping only, but neglected the interaction between dike reliability, land subsidence and flood risks, thereby likely either overestimating or underestimating future risks. The transferrable framework presented herein contributes to more robust risk assessments for other global delta cities facing significant relative SLR and flooding challenges.

2. Methods

2.1. Seawall Deformation Prediction

We apply a Differential Synthetic Aperture Radar Interferometry (DInSAR)-based geotechnical model developed by Pepe et al. (2016), Yin et al. (2019), and Zhao et al. (2015) to predict the cumulative deformation of seawall (i.e., sea dike) along the Shanghai coastline. First, we use multitemporal and multisatellite synthetic aperture radar (SAR) images to retrieve the seawall deformation history and rates in Shanghai. The first data set consisted of 35 SAR images, acquired by the C-band ENVISAT ASAR sensor on the ascending orbits from 26 February 2007 to 13 September 2010. And the second data set comprises 33 SAR images, acquired by the C-band Sentinel-1A sensor with ascending passes from 1 August 2015 to 17 February 2019. All available SAR data are processed with the small baseline subset (SBAS) technique, which is a well-established advanced time series DInSAR algorithm (Berardino et al., 2002; Lanari et al., 2007). The approach has been validated through the cross comparison between the leveling and the SBAS measurements of seawall subsidence during the same time period (Zhao et al., 2015). A time-dependent geotechnical centrifuge model (Yang et al., 2008), which was established for Shanghai based on laboratory tests, has indicated that dike deformation due to self-weight consolidation is a nonlinear process that could last for decades. We then adopt the satellite DInSAR-based measurements to constrain the laboratory-derived geotechnical model. Hence, the DInSAR-based geotechnical model enables exploration of the temporal evolution of the asymptotic seawall deformation. This is theoretically calculated over a time period from the baseline 2010 to the end of the consolidation phase (2050) (Figure S1 in the supporting information).

2.2. Seawall Reliability Analysis

We investigate the geometry of typical seawall structures and assume that wave overtopping is the main failure mechanism for potential sea dike breaching in Shanghai. In theory, wave overtopping can be described by a limit state function, in which the “load” is the actual wave overtopping rate. The “strength” is a critical rate for erosion of the landward slope of the dike. The reliability function is expressed by

$$Z = q_{adm} - q \quad (1)$$

where Z is the limit state, q_{adm} is the admissible wave overtopping rate (L/m/s), and q is the actual wave overtopping rate (L/m/s). The actual overtopping rate is calculated through an empirical overtopping function for sea dikes with crown walls recommended by Chinese Guideline of Sea Dike Design (GB/T 51015-2014):

$$q = 0.07^{R_c/H_s} \exp\left(0.5 - \frac{b_1}{2H_s}\right) BK_A \frac{H_s}{T_p} \left[\frac{0.3}{\sqrt{1/\tan\alpha}} + \text{th}\left(\frac{d}{H_s} - 2.8\right)^2 \right] \ln \sqrt{\frac{gT_p^2}{2\pi H_s \tan\alpha}} \quad (2)$$

where KA is the influence factor for roughness on the slope, and this value is suggested as 1.0, 0.49, 0.4, and 0.5 followed by the material of revetment made by concrete slab, riprap, dolos, and hollow square, respectively; H_s is the significant wave height (m) at the toe of the structure; d is the water depth (m) at the toe of the structure; g is the gravity acceleration (m/s²); T_p is the peak period (s); $\tan\alpha$ is the outer slope angle; R_c is the crest freeboard (m); b_1 is the distance from the crown wall on the crest to the seaward (m); and B is an empirical factor; this value is suggested as 0.6, 0.25, and 0.38 when the value of $\tan\alpha$ is 1/1.5, 1/2, and 1/3, respectively. The wave data (H_s and T_p) were retrieved from a modeling repository with hourly output interval for 1960–2018 (Figure S2). This wave modeling system is built on the unstructured grid SWAN

model (Ge et al., 2013), which is driven by National Centers for Environmental Prediction reanalysis wind data from 1960 to 1979 and European Centre for Medium-Range Weather Forecasts Re-Analysis-Interim data from 1980 to 2018.

We assume that all seawalls are well maintained, at the first layer of revetment, with (good quality) grass on the dike inner slope, and geobags are filled with clay and covered by plastic bags as the second layer underneath the grass (see typical cross section of Shanghai seawall in Figure S3). The admissible overtopping rate is defined based on different revetment materials placed on the inner slope of the dike according to Chinese Guideline of Sea Dike Design (GB/T 51015-2014). Accordingly, it is assumed that the grass cover will be damaged/eroded during an overtopping discharge rate of more than 10 l/m/s (EurOtop, 2016). When this wave overtopping occurs, it possibly causes structural failure and further leads to potential seawall breaching. In this study, we determine the location and width of seawall breaches along the coast of Shanghai using the recommended values for wave overtopping threshold (~20 l/m/s), which are derived from a large number of wave flume experiments (Zhang et al., 2017) and proposed by the National Guidelines of Marine Disaster Risk Assessment for the evaluation and anticipation of dike failures in China.

2.3. Floodwall Reliability Analysis

Overtopping/overflowing is considered as the most common failure mode for the floodwall (i.e., river dike) along Huangpu River. Other failure mechanisms, such as instability due to sliding and failure due to seepage under the walls, could also be relevant. However, given the configuration of floodwalls and soil structure in Shanghai, these mechanisms are considered less likely (Wang, 2016). It is assumed that all floodwalls along Huangpu River behave as L walls with enough self-weight or sufficient pile capacity to resist monolithic sliding or overturning, leaving only concrete fracture and rebar bending as the possible failure mechanism. For the existing I walls (cantilever walls), we assume that the ground on the dry side of the wall is paved with concrete or asphalt, so that overflow scour is not a possible failure mode. In order to calculate overflow/overtopping volume, the proposed equations are defined as

$$Z = q_c - q \quad (3)$$

when

$$z_0 \leq z_c - \Delta l, q = m_{os} \cdot \sqrt{g(H)^3} \cdot \exp\left[-3 \frac{(z_c - \Delta l - z_0)}{H}\right] \times 1,000 \quad (4)$$

when

$$z_0 > z_c - \Delta l, q = \left[m_{ol} \cdot 0.55 \sqrt{-g(z_c - \Delta l - z_0)^3} + m_{os} \cdot \sqrt{g(H)^3} \right] \times 1,000 \quad (5)$$

where Z is the limit state, q_c is the critical discharge (L/m/s), q is the average overflow/overtopping discharge (L/m/s), H is the significant wave height (up to ~0.7 m), z_c is the crest level (m), z_0 is the local water level (m), Δl is the land subsidence (m), g is the gravitational acceleration (9.81 m/s²), m_{os} is the model factor overtopping ~log N (0.34, 0.09²), m_{ol} is the model factor flow ~ N (1.1, 0.3), and N represents the normal (Gaussian) function with the values in parenthesis representing the mean and standard deviation. Based on a similar case of flood defenses in New Orleans, a deterministic value of 10 l/m/s is used as the critical threshold for this case (EurOtop, 2016).

Another predominant failure type, the collapse of floodwall caused by high water pressure is further specified along Huangpu River. A typical pattern of structure strength failure for floodwall can be defined as the moment when steel rebar in the concrete rupture under the load of extraordinary water level (Figure S4). In light of this, the simple form of a reliability function can be described as follows:

$$Z = M_r - M_l \quad (6)$$

where Z is the limit state, M_r is the resistant moment ($N \cdot m$), and M_l is the moment loading on the wall ($N \cdot m$). M_r can further be represented by variables related to floodwall structure, and M_l can also be expressed using several parameters of water loading.

$$M_r = \frac{0.87f_y h_{wall} A_s}{1.7} \times \frac{1}{1,000} \quad (7)$$

$$M_l = \frac{1}{6} \rho_w g [z_0 - (z_l - \Delta l)]^3 \quad (8)$$

where A_s is the actual steel cross-sectional area used in the floodwall (mm^2), ρ_w is the water density ($1,000 \text{ kg/m}^3$), g is gravitational acceleration (9.81 m/s^2), z_0 is the water level (m), z_l is the ground level (m), Δl is the land subsidence (m), f_y is the tensile strength of steel (N/mm^2), and h_{wall} is the thickness of the floodwall (mm).

2.4. Flood Inundation Modeling

We use a simplified 2-D flood inundation model (FloodMap-Inertial) to simulate dike failure-induced flooding and to derive inundation maps. The model assumes that the coastal/river floodplain is protected by a continuous, broad-crested embankment through which water flow exchange occurs between the sea/channel and hinterland. A simplified solution has been adopted in the model for the treatment of overland flood routing in a raster-based environment. This solves the 2-D shallow water equations using a computationally efficient inertial algorithm (Bates et al., 2010), with the Forward Courant-Freidrich-Levy Condition approach to the calculation of the time steps. A full description of the model structure and parameterization can be found in Yu and Lane (2011). FloodMap-Inertial, as well as its earlier diffusion-based version (FloodMap) (Yu & Lane, 2006), have been tested and implemented in fluvial, pluvial, and coastal environments in Shanghai (Yin et al., 2013, 2015, 2019), achieving a good level of performance for flood prediction. A recent validation study (Yin et al., 2016), comparing model output against observed inundation in New York City, further indicated that the city-scale and street-level modeling framework similar to that used here is capable of high predictive skill for inland flooding.

Floodplain topography and flow boundary conditions are used as inputs to drive the flood modeling. A city-wide digital elevation model (DEM) constructed from 0.5-m interval contour lines is available, with a horizontal resolution of 50 m and a vertical accuracy of 0.1–0.2 m. Moreover, a finer-resolution (5 m) DEM of the financial center, Lujiazui, generated by Shanghai Municipal Institute of Surveying and Mapping using photogrammetric technology, is employed for street-level inundation modeling. The potential breaching segments identified in the reliability analysis are completely removed, while the remainder of the dike system remains the same. The heights of remaining flood defenses under the current and future situations are then overlaid onto the original “bare earth” DEMs. Still water levels with various return periods along the coast and Huangpu River are obtained through linear interpolation from station-based flood probability analysis conducted by Shanghai Water Authority in the last decade (Table S1 and Figures S2g–S2i). It should be noted that flood probability, particularly for high return periods (e.g. 1,000-year), could be highly uncertain with limited length (decades to a century) of still water observations (Figure S5). Assuming tidal cycles remain constant, dynamic boundary conditions (time series of water levels) are generated for 10-, 100-, and 1,000-year flood scenarios, by proportionally scaling the stage hydrographs recorded at the boundary gauge stations during Typhoon Winnie (the worst case in history). To account for plausible increases in sea level, we combine the current level of flood frequency with relative SLR projections, enabling future flood scenarios to be formulated. Considering the semidiurnal nature of the tide, a 2-day (48 hr) tidal cycle including four rising phases and four falling limbs is applied in the flood simulations. An empirically based, relatively high floodplain roughness coefficient (Manning's $n = 0.06$) is used in the modeling to represent the effect of urban features (e.g., buildings) on overland flood routing.

3. Results

3.1. Relative SLR Projections

Sea level change varies regionally to a significant degree, primarily due to local contributing factors such as vertical land movements, changes in oceanic currents, variations in atmospheric pressure, and static equilibrium processes. A global data set from Kopp et al. (2014) provides the probabilistic, localized SLR projections at Lvsj gauge station located in Yangtze River Delta, under three Representative Concentration Pathways (RCP 2.6, RCP 4.5, and RCP 8.5). The projections take into account the key contributing components of sea level rise, including ice sheet melting, glacier and ice cap melting, oceanographic processes

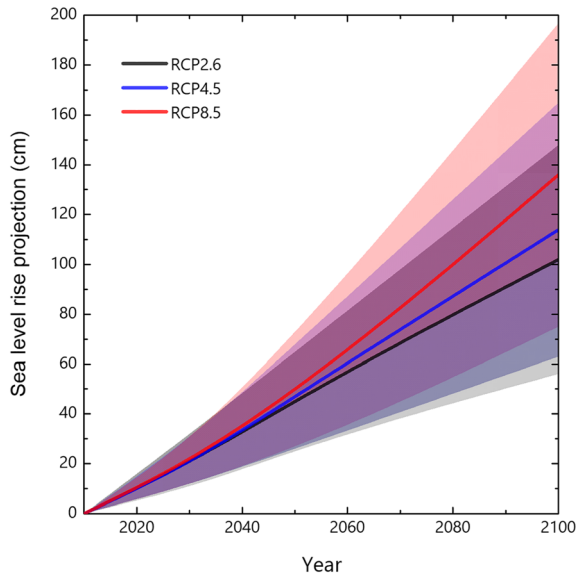


Figure 1. Projected relative SLR under three RCPs for the city of Shanghai. The shadow area represents the range of uncertainty (5th–95th percentile) for each prediction.

(e.g., thermal expansion of ocean water), land water storage, and non-climatic local effects such as glacial isostatic adjustment and subsidence. Site-to-site differences in local SLR projections are fundamentally dependent on varying nonclimatic land subsidence. Hence, the relative SLR in the present study are estimated by incorporating the climatically driven absolute SLR decomposed from the projections at Lvsj station and the linear approximation of future subsidence rate (6 ± 1 mm/year) in Shanghai (Yin et al., 2013). The latter is based on city-wide leveling measurements since 2000 and the long-term target of subsidence control. All relative sea level projections by 2100 are given with respect to the baseline year of 2010.

The local or relative SLR projections for Shanghai are presented in Figure 1. Projected local sea levels and associated uncertainty ranges rise progressively through the 21st century under the climatic and anthropogenic forcing. The projections show a markedly higher rise and substantially wider range in local sea level than the more conservative estimates of the State Oceanic Administration derived from trend extrapolation of long-term tide gauge records (State Oceanic Administration People's Republic of China, 2016). By 2030, all three pathways could have a median (50th percentile) rise of 21–22 cm in relative sea level. By the year 2050, the median relative SLR is projected to be 45 cm under RCP2.6 and 50 cm under RCP8.5, with nearly

equal contributions from both climatic and nonclimatic (subsidence) factors. We found that the effect of climatic forcing on relative SLR exceeds the local effect of background subsidence in the late 21st century. Due to growing contributions of atmospheric and ocean warming to SLR, differences among the three emission scenarios become more pronounced toward the end of the century, with local relative SLR (5th–95th percentile) ranging from 56 to 148 cm for RCP2.6, 63 to 165 cm for RCP4.5, and 75 to 197 cm for RCP8.5. The greatest contributions to the median outcome are from oceanic thermal expansion, followed by glacier and ice cap melting. The Antarctic ice sheet is projected to contribute most to the broad uncertainty ranges of future SLR.

3.2. Dike Failures Along the Coast and River

Flood levels with various return intervals (10-, 100-, and 1,000-year) for the present and future scenarios are used to evaluate the reliability of seawalls along the coast and floodwall along the Huangpu River (Figure 2). Overtopping and breaching (caused by overtopping) are considered as the two main failure mechanisms for seawalls in Shanghai. Seawall breaching is defined to occur when the overtopping discharge is in excess of 20 l/m/s (see more details in section 2). As is shown in Figure 3, the locations of seawall failures under a hydraulic load (water level and wave height) of current 10-year return period (RP) are sparsely distributed in the very limited weak sections of seawalls, mostly in the Yangtze River Estuary. During a 100-year event, both failures could simultaneously occur along the coast of Baoshan and southwestern Chongming island, as the existing low-level seawalls in these periurban and rural areas are considerably lower than the design 100-/200-year RP protection standard. Additionally, all sections of seawall in Fengxian are predicted to be overtopped, largely due to significant wave heights (2–3 m) in Hangzhou Bay (Figure S2). The failure locations further extend to Jinshan district, parts of Pudong and Hengsha islands, and northeastern Chongming island during an extreme 1,000-year of RP event, accounting for approximately 40% of the total seawall length (508 km). Compared to the 10-year RP event under 2010 relative sea level, the overtopped and breached seawall length increases by 1 and 3 times, respectively, for 100- and 1,000-year RP events.

With the effects of sea level rise and land subsidence, still water levels would increase proportionately at all return periods. Under the RCP 8.5 scenario, the current 10- and 100-year flood levels in Shanghai could be exceeded approximately twice more frequently in 2030, 3–5 times more frequently by 2050, and over 50 times more frequently with a 136-cm rise in relative sea level (50th percentile) by the end of the 21st century (Figure S6). Increasing flood levels and seawall deformation (Figure S1), in turn, could increase the likelihood of seawall failures over time. However, the percentage increase is notably greater for the shorter

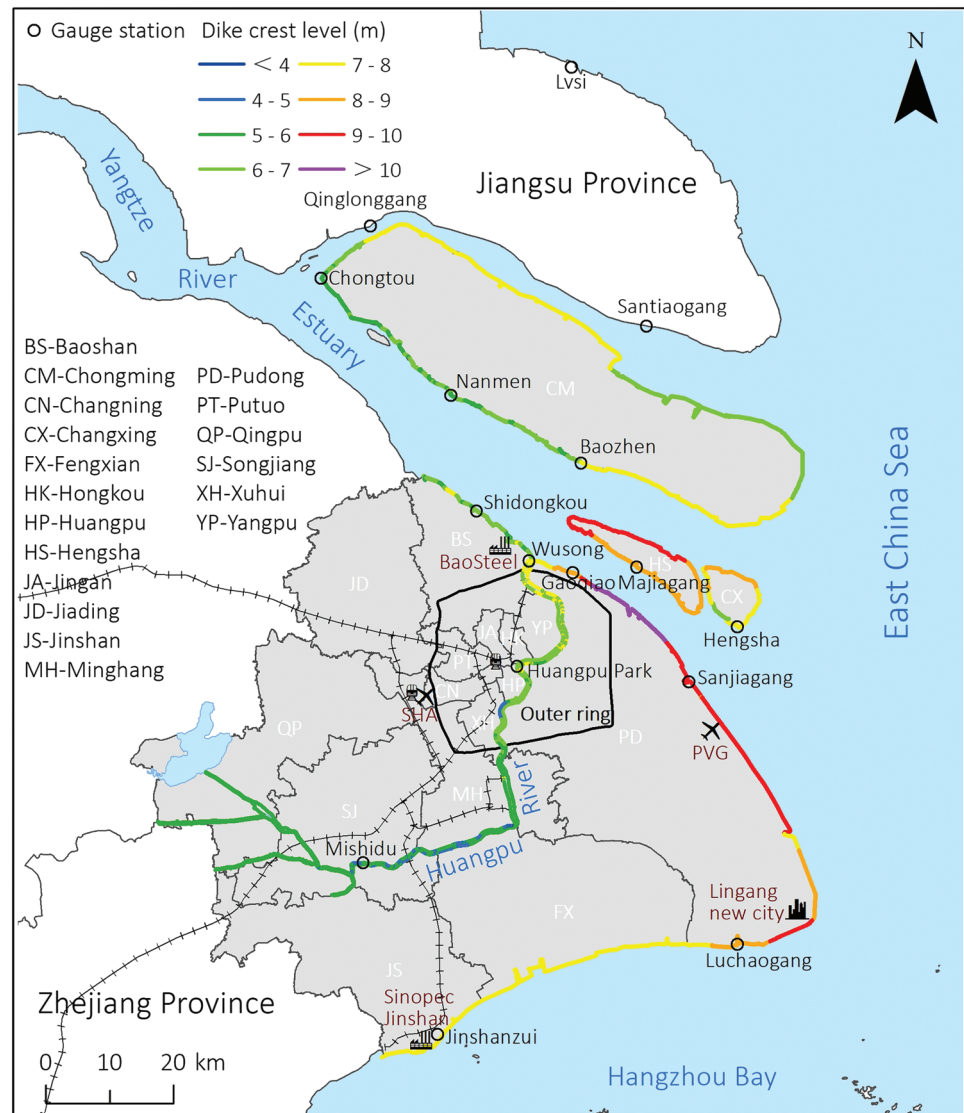


Figure 2. The geographical location of completely enclosed dike system, tide gauges, and critical infrastructures/facilities in Shanghai and the Yangtze River Delta. The city center lies within the outer ring (highway). The crest heights of seawalls and floodwalls above Wusong Datum were obtained from leveling measurement campaigns by the municipal authority in the 2010s.

return period (more frequent) events. For example, the central estimate (50th percentile) of the length of overtopped seawall is increased by 940%, 39%, and 3.6% under return periods of 10-, 100-, and 1,000-year, respectively, in 2030 compared to 2010. There are no major differences in terms of seawall failure location and length affected/breached between RCP2.6 and RCP 8.5 scenarios, for 2030, 2050, and 2100. By 2100, the potential overtopped and breached sections account for 71% and 67%, respectively, of total seawall length under the RCP8.5 scenario during a flood of 1,000-year return period (Table 1). However, the majority of the seawalls in Pudong are expected to be able to withstand overtopping and breaching until later in the 21st century, even when subject to a hydraulic load of 1,000-year RP. This is due to the relatively high quality of seawall (i.e., crest height, berm height, and crown wall) and comparatively low hydraulic loads (i.e., storm tide and wave height) (Figure S2). Pudong district is a state-level newly developed area with much critical infrastructure and pilot economic zones, such as Pudong airport, Port of Waigaoqiao, Shanghai free-trade zone, and Lingang new urban area (Figure 2). Therefore, higher safety standards (i.e., more than 1 in 200 years) were implemented in this district.

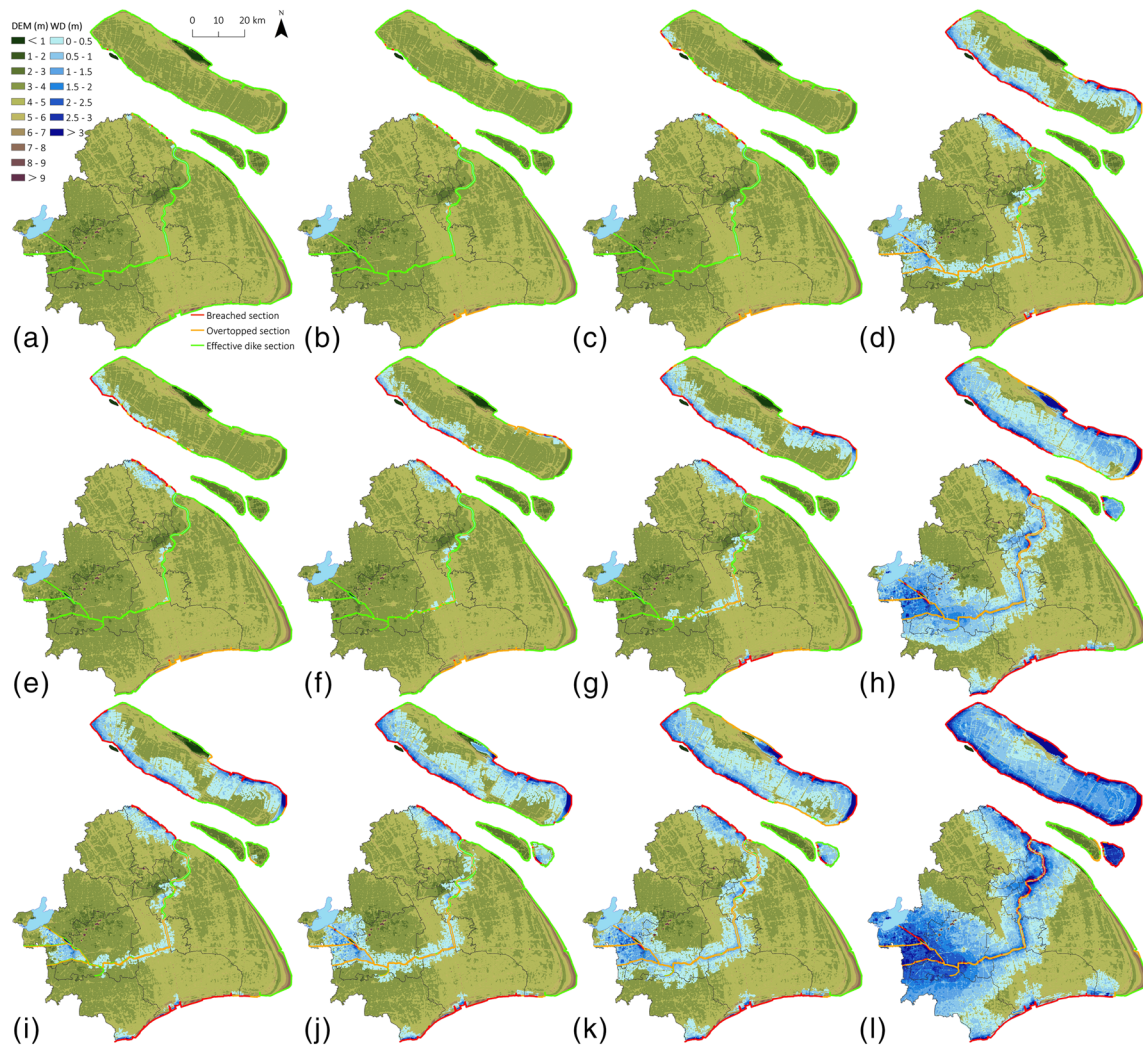


Figure 3. Projected central estimates (50th percentile) of dike failures and flood inundation under present and future scenarios (RCP 8.5) in Shanghai. (a–d) Ten-year flood in 2010, 2030, 2050, and 2100. (e–h) One hundred-year flood in 2010, 2030, 2050, and 2100. (i–l) One thousand-year flood in 2010, 2030, 2050, and 2100.

Overtopping/overflowing and structural failure due to high river water levels are regarded as the two main failure mechanisms of floodwalls along the Huangpu River (see more details in section 2). In terms of overtopping/overflowing, this floodwall can withstand a 100-year RP event under the current condition (2010), with only two potential failure locations on the left bank of the Huangpu River's middle reach. For the 1,000-year RP event, wave overtopping and overflowing spread to the upstream reach and the right bank of the Huangpu River (Figure 3), with additional failures scattered throughout the middle reach. Under future relative SLR in 2030, 2050, and 2100, the floodwall could be overtopped under a 10-year RP flood, even in an optimistic RCP2.6 scenario (Table 1). In addition to the middle reach, the floodwall in the upstream reach of the Huangpu River cannot withstand the hydraulic load of a 1,000-year RP event with 2030 sea level, while the downstream reach is far safer except for the 1,000-year RP event under the RCP 8.5 scenario (then entirely overtopped). This can be explained by the lower standard of protection level (1 in 50 years) and lower socio-economic development in the upstream reach than in the middle and downstream reaches (protection level of 1 in 1,000 years). Risks along the middle reach of the Huangpu River (comprised of downtown districts) are exacerbated by ongoing engineering projects (e.g., massive high-rise construction and underground space exploitation), which are causing land subsidence and floodwall deformation. With projected sea level rise until 2100, almost the entire floodwall system along the Huangpu River could be overwhelmed, especially during 100- and 1,000-year RP events.

Table 1
Predicted Length of Dike Failure and Extent of Flood Inundation Under Current and Future Scenarios (RCP 2.6 and 8.5)

Scenarios	10-year flood event			100-year flood event			1,000-year flood event		
	O(10 ² km)	B(10 ² km)	F(10 ² km ²)	O(10 ² km)	B(10 ² km)	F(10 ² km ²)	O(10 ² km)	B(10 ² km)	F(10 ² km ²)
2010	0.04/0.01	0.01/0	0.07	1.13/0.07	0.46/0	1.77	2.20/1.54	2.00/0.01	10.21
2030 RCP 2.6	0.36/0.04	0.02/0	0.16	1.56/0.19	0.67/0	3.04	2.28/2.52	2.14/0.02	15.39
2030 RCP 8.5	0.39/0.04	0.03/0	0.17	1.58/0.19	0.68/0	3.09	2.28/2.53	2.14/0.02	15.79
2050 RCP 2.6	0.72/0.05	0.12/0	0.61	1.72/0.65	1.30/0	6.21	2.67/2.82	2.23/0.07	20.29
2050 RCP 8.5	0.77/0.05	0.15/0	0.80	1.76/0.71	1.38/0	6.88	2.89/2.98	2.26/0.08	21.69
2100 RCP 2.6	1.34/0.85	0.59/0	3.13	2.19/2.77	1.81/0.07	18.17	3.37/3.20	3.18/0.29	36.67
2100 RCP 8.5	1.73/2.43	1.23/0.01	11.27	2.74/3.13	2.24/0.15	28.92	3.63/3.20	3.40/0.54	42.07

Note. O, B, and F represent overtopped length, breached length, and flooded extent. Values on both sides of the slash for O and B are failure lengths of seawall and floodwall, respectively. The median estimates (50th percentile) of failure length and flood extent are presented for future RCP 2.6 and 8.5 scenarios.

In terms of breaching due to structural failure, the floodwall along the Huangpu River is expected to remain intact under the 100-year RP event until 2050, while dike breaching could occur at two locations in the upstream reach of the Huangpu River during the 1,000-year RP event with the baseline sea level (2010). Breaching further spreads to other sections of the upstream reach in the year 2030 and sparsely affects the downstream reach (Figure 3). In contrast to the prevalence of overtopping, the middle reach of the Huangpu River could experience very little structural failure under a 100-year RP event until the end of this century, due to the minor effect of small waves (0.3–0.7 m) along the river. Overall, under a 1,000-year RP event with scenario RCP 8.5 in 2100, the average very likely estimates (5th–95th percentile) of breached floodwall length range from 14.17 km (3%) to 233.26 km (49%), indicating large uncertainties in the long-term projections.

3.3. Evolving Flood Hazards Throughout the City

Inland flood inundation induced by overtopping and dike breaching is simulated using a 2-D hydrodynamic model with a fine-resolution city-scale DEM (see more details in section 2). As examples, Figure 3 and Table 1 also illustrate the central estimates (50th) of predicted city-wide maximum inundation (extent and depth) for three representative return periods (10-, 100-, and 1,000-year) under current and future scenarios. An immediate finding is that the failure-induced flood inundation, as expected, increases significantly for longer return period events. The general patterns of inundation, however, depend on the interplay among flood levels, failure modes, and topographic characteristics. For the present sea level, almost no inundation can be observed during a 10-year RP flood event, except negligible ponding (0.1% of the total area), mostly in the coastal floodplain of Baoshan district. Under the contemporary 100-year flood level, low-lying waterfront areas in Baoshan and southwestern Chongming island are likely to be inundated without high standard seawalls. By contrast, overtopping failures along the Fengxian coast result in no inland flooding, due to the very limited amount of discharge over the crest of the seawall. Additionally, marginal inundations with shallow water depth may occur in only the hinterland protected by the remarkably low-level floodwall sections. For the extreme 1,000-year RP event, flood inundation tends to be deeper and more extensive compared to 100-year event, affecting the densely populated areas and several economically important functional zones such as Baosteel Group and Sinopec Shanghai Petrochemical Company (Figure 2). Overland flow through breached seawalls could inundate over 45% of Chongming island and intrude further inland to Baoshan, with maximum water depths exceeding 3 m. Flooding extends from the low lands of the upstream catchment to both banks along the middle reaches of the Huangpu River floodplain. Because of the presence of topographic confinement on the coastal plain, inland flow caused by seawall breach is restricted to very limited portions of coastal areas along Hangzhou Bay.

A cross comparison of the derived flood hazard maps in Figure 3 further reveals that the relative SLR could lead to a nonlinear increase in future inundation of the delta city. The severity of flood extent is determined by the rate of projected relative SLR and is more pronounced at shorter return periods. When a 0.22-m rise (median) in the local sea level by 2030 is considered, the total inundation area is projected to increase by 123%, 75%, and 55% relative to 2010 for 10-, 100- and 1,000-year RP event, respectively. Spatially, the inundation patterns are characterized by a high degree of consistency between the present and 2030 scenarios.

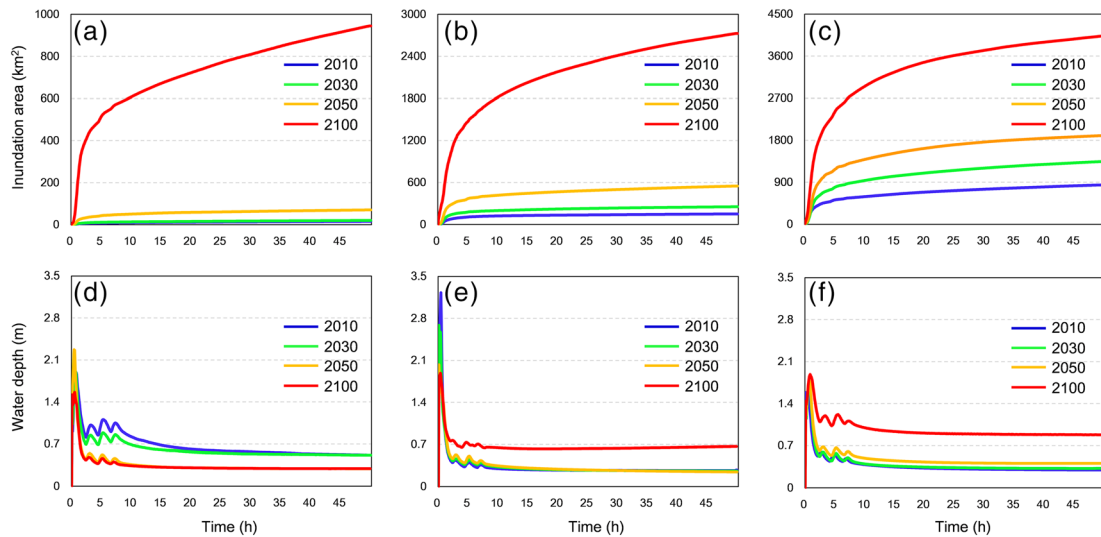


Figure 4. Time series of projected inundation for various RP events under present and future scenarios (RCP 8.5) in Shanghai. (a–c) Predicted wet areas with the difference in y axis scaling for 10-, 100-, and 1,000-year floods. (d–f) Average water depths for 10-, 100-, and 1,000-year floods.

However, there is a marked difference in Hengsha (Figure 3j) where 1,000-year RP flooding affects only a small portion of dike-protected hinterland under present conditions but could inundate most of the island through a 3.5 km long breached seawall by 2030. With a median relative SLR of 0.5 m under RCP8.5 projected by 2050, flood extent and depth for each return period are expected to increase drastically in the coastal and Huangpu river floodplains. The inundated area is projected to be more than double for the 1,000-year flood extreme and increase more than tenfold for the 10-year RP event when compared to 2010. Meanwhile, the projected SLR could contribute to a 53% and 18% rise in the average water depth for the 10- and 1,000-year RP flood scenarios, respectively. If the relative sea level is raised by 1.36 m in 2100, the flood impact of the 10-year return period storm could even exceed that of the 1,000-year return period at the 2010 baseline sea level. Without timely adaptation measures, 1,000-year RP flooding could overwhelm the delta city by the end of this century (Figure 3l). Under this scenario, more than 4,200 km² (62% of the total area) of the city could be flooded with an average inundation depth of 1.2 m. The most susceptible areas to the magnified flood hazard are Chongming island and the Huangpu River floodplain including the city center, where the inundation distance exceeds 10–20 km inland. Overall, the implication is that Shanghai with a population of 24 million, though relatively safe from flooding today, will become increasingly risk prone due to SLR and subsidence.

Figure 4 shows the time evolution of projected inundation (extent and depth) for each scenario. It is noted that the time series are consistent with each other, suggesting a similar pattern of inundation process during each simulation. Results also indicate that the temporal development of flood inundation is not synchronous with the timing of the tidal cycle. In each case, both the flooded area and depth rapidly increase during the rising phase (the first 1–3 hr) and then storm water progressively extends overland shortly after the flood peak (up to 10 hr). Afterward, a steady state of inland flooding is attained as the stage subsides. The inundation area continues to slightly increase, but the average water depth generally remains constant until the end of the model run. This is explained by Shanghai's low-lying floodplain with a downward topographic gradient away from the shore. Moreover, SLR exerts varying degrees of influence on the 10-, 100-, and 1,000-year RP flood scenarios. More frequent (short-RP) flood events, in terms of inundation area (Figures 4a–4c), are affected more by SLR than those with longer return periods, confirming what is shown in Figure 3. On the contrary, the SLR effect on the inundation depth is predicted to increase from the 10-year RP event to extreme 1,000-year RP flood (Figures 4d–4f). An important finding is that the time depth curves for the 10-year floods even show a significant decrease in average water depths from 2010 to 2100, because the increase in the 10-year flood levels due to SLR essentially translates into larger inundation areas in the extensive floodplain rather than greater water depth. In general, flood hazards are expected to be more destructive as sea level rises, with not only greater inundation but also longer duration (days to weeks).

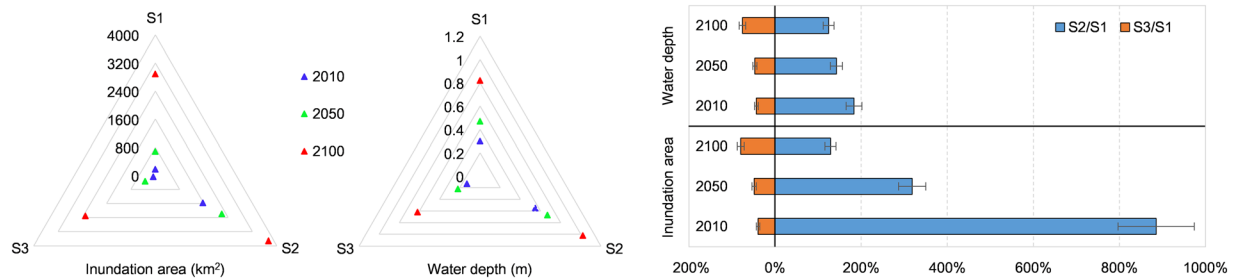


Figure 5. A comparison of predicted 100-year flood inundation (extent, depth, and percentage difference) between methods considering failure probabilities (S1), assuming complete failure (S2), and assuming only overtopping (S3) by 2010, 2050, and 2100 (RCP8.5).

4. Discussions

This study demonstrates the growing dependency of delta cities' flood safety on the level of flood protection and thus reveals the importance of incorporating sophisticated reliability assessment into delta flood risk analysis at a local, city level. Using Shanghai as a case study, for the first time, we have demonstrated how the vulnerability of an existing dike system in a delta city will develop over time assuming different SLR scenarios and how dramatically the compound flood hazards may increase over time. Notably, rising seas increase dike failures and flood hazards locally, with the highest and lowest impacts in the Yangtze River Estuary and Hangzhou Bay, respectively. We also found that the projected SLR would substantially amplify the cascading effect generated by not only smaller floods, which cause little threat of failure and inundation at the current state, but also extreme events, which may repeat the tragedy of New Orleans in Shanghai by the end of the 21st century, without additional adaptation measures.

Although the vulnerability of delta cities to rising seas is well known, our findings on the effects of the relative SLR on failure-induced flooding are comparable with those of previous studies. For example, Wang et al. (2012) projects that SLR and land subsidence could result in 46% of dikes being overtopped and half of the city being flooded by a Winnie-like storm surge in 2100. Projections from Du et al. (2020) indicate that a 1,000-year flood is likely to inundate 76% of mainland Shanghai under the RCP8.5 scenario of relative SLR by the end of the 21st century. The studies only accounted for overtopping on the basis of design protection level, or dike breach with an assumption of complete failure of defense structures. However, our study advances these earlier assessments by including empirically derived dike failures based on reliability analysis (the compound effects of both overtopping and dike breach using actual seawall and floodwall heights) in flood modeling and soil subsidence in estimating relative SLR. Using 100-year flooding as an example, we find that the predicted inundation area and water depth are 61% and 57% higher than those with only overtopping scenario (S3) but 785% and 83% smaller than those with complete failure scenario (S2) in 2010 (Figure 5 and Figure S7). The difference between each approach is expected to decline gradually to $\pm 20\text{--}30\%$ with SLR until 2100. Thus, the case of Shanghai shows that flood risks in major delta cities are very likely to be poorly estimated, as most current flood risk modeling regularly used S2 or S3 approaches and neglected the effect of dike reliability.

Schubert and Sanders (2012) demonstrated that the best method for a particular application of 2-D flood inundation model will depend on available data, computing resources, time constraints, and the specific modeling objectives. We realize that a coarse resolution (50 m) DEM is insufficient to capture intricate flow paths in urban topography and tends to be biased in the predicted inundation patterns of downtown Shanghai. Street-level inundation modeling in Lujiazui District is thus performed and then compared with city-scale modeling (Figure 6). The general pattern of street-level inundation is similar to what has been reported at city scale. However, flood inundation is overestimated in the city-scale modeling as detailed surface features represented by high-resolution DSM may block specific hydraulic connectivity. With the increase in flood magnitude, the differences of flood inundation (extent and depth) between street-level and city-scale simulations reduce slightly. Results agree with previous studies (e.g., Yin et al., 2016) that high-resolution DEM is essential for resolving flood patterns in an urban setting.

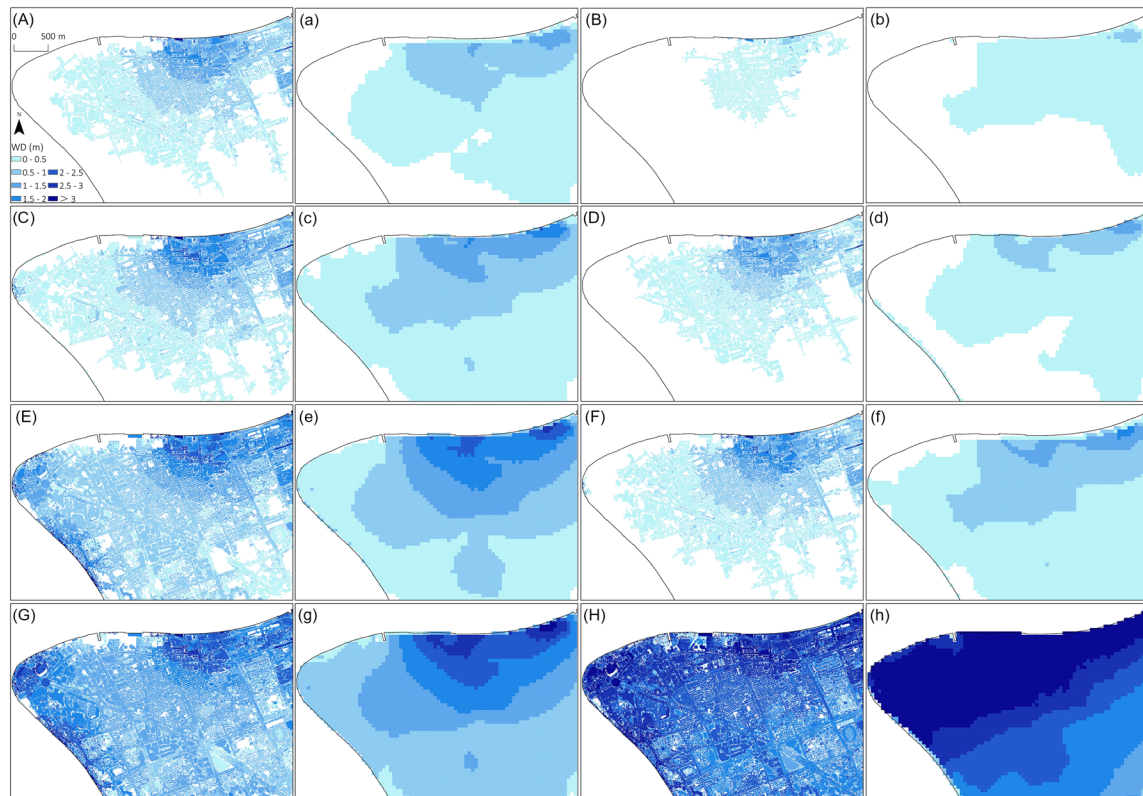


Figure 6. A comparison of street level (5-m resolution, A–H) and city-scale (50-m resolution, a–h) inundation modeling in Lujiazui, Shanghai; (A/a) 1,000 years in 2010, (B/b) 100 years in 2030, (C/c) 1,000 years in 2030, (D/d) 100 years in 2050, (E/e) 1,000 years in 2050, (F/f) 10 years in 2100, (G/g) 100 years in 2100, (H/h) 1,000 years in 2100.

We acknowledge that there are several limitations to our analysis. The most important is that future changes in storminess are not considered in our study. Although previous research has indicated that an increase in extreme high water levels for the historical period is due almost exclusively to SLR rather than storm climatology changes (Menéndez & Woodworth, 2010; Zhang et al., 2000), the effect of enhanced storminess is found to be more pronounced in the late 21st century (Li et al., 2018; Lin et al., 2012; Lin & Emanuel, 2016). It is yet unclear how climate change might affect the frequency and intensity of tropical cyclones and associated flooding in the Yangtze River Delta. Including the climatological-hydrodynamic modeling of probabilistically based synthetic events under future climate conditions is computationally expensive and beyond the scope of this study. Further research could quantify the compound impacts of both SLR and storm climatology change on future flood hazards locally. Moreover, we neglect the nonlinear interactions between SLR and extreme water level, which is dominated by tide-surge-wave, intense rainfall induced pluvial flooding, and river flooding in deltas and estuaries (Moftakhari et al., 2017; Ward et al., 2018). Although the linear superimposition of SLR and the flood return levels has been used in many coastal flood vulnerability studies, sea level variations could affect the tidal range, storm surge, wave height, and river discharge separately in some regions (Arns et al., 2020; Devlin et al., 2017; Wahl, 2017). Storm surge, high tide, heavy rainfall, and upstream river flooding are the four major drivers of extreme water levels along Shanghai coast and Huangpu River. Catastrophic flooding tends to be triggered when three or four of these drivers occur simultaneously. Fully accounting for all the drivers and their nonlinear interactions requires an integrated modeling framework that could be addressed in future assessments. Finally, the empirical dike reliability functions used in this study are uncertain for Shanghai, as large-scale dike failures have not occurred since the early 2000s when the continuous and high standard seawall/floodwall system along the coast and river was completed. These engineering works followed the devastating flooding in Shanghai by Typhoon Winnie in 1997. The empirically based dike reliability analysis can still hold because sensitivity analysis allows quantification of the uncertainties in each component and their combination.

Taking into account the above uncertainties and limitations, the dike failure-induced compound inundation predicted by reliability analysis and hydrodynamic modeling (see section 2) could be applied to assess increasing flood risks and to prioritize site-specific adaptation efforts at city scales. Typically, with available probabilistic flood hazard footprints to 2100, annual expected damages to populations and assets in the delta city may be evaluated under both present and future conditions. Our analysis combined with cost-benefit assessment (Ruig et al., 2019) can be further used to identify areas where investments in protective measures should be prioritized and to identify tipping points when (new) adaptation options should be emphasized, thus providing a strong basis for maintenance and/or improvement of the optimal protection standard along the coast and river. Particularly, a movable barrier system at the mouth of Huangpu River (like the Thames Barrier for London and the Maeslantkering Barrier for Rotterdam) should be considered for Shanghai. Such an investment might be more economically effective in the long term, as the city's 479.7-km floodwalls would need to be raised every decade due to relative SLR, in the absence of a storm surge barrier. Another urgent action is upgrading of the low-level seawalls (typically 5–7 m above Wusong Datum) along the coasts of Baoshan and Chongming and regular maintenance of the high-level seawalls in Pudong and Changxing. Our modeling, in terms of timing, can also support evacuation zoning and emergency planning for possible contingencies. Besides applications of flood risk management in Shanghai, the methodology demonstrated herein is readily transferable to other deltaic cities around the world such as Tokyo, Bangkok, and Jakarta, where the rate of SLR and subsidence are accelerating, adding to the area below sea level. Such detailed studies performed elsewhere would be essential for developing sustainable flood resilience plans, which aims to offset the effect of rising sea and to prevent delta cities from drowning before the trends become irreversible. Ultimately, massive projects such as the Dutch polder systems may be feasible for wealthy megacities on sinking deltas but are unaffordable for many delta cities in the developing world. Difficult strategic choices on which area to preserve and which to abandon will arise because the time window to sustain deltas is closing gradually (Day et al., 2016).

Competing Interests

The authors declare that they have no competing interests.

Data Availability Statement

Data sets for this research are available through Ge et al. (2013) and Wang et al. (2018).

Acknowledgments

This work was supported by the National Key Research and Development Program of China (Grant 2018YFC1508803, 2017YFE0100700, 2017YFE0107400), the National Natural Science Foundation of China (Grant 41871164, 51761135024), the National Social Science Fund of China (Grant 18ZDA105), the Research Projects of Science and Technology Commission of Shanghai Municipality (Grant 19DZ1201500, 18ZR1410800), the Fundamental Research Funds for the Central Universities (Grant 2018ECNU-QKT001, 2017ECNUKXK013), and Institute of Eco-Chongming (Grant ECNU-IEC-202001). N. L. has received funding from the National Science Foundation of the United States (Grant EAR-1520683). D. P. Y. and R. L. W were funded by the UK Natural Environment Research Council (Grant NE/R009600/1, NE/S017186/1). B. J., J. B., and Q. K. acknowledged financial support from the Netherlands Organization for Scientific Research (NWO) (Grant ALWSD.2016.007). Q. Z. has performed within the ESA-MOST Dragon 5 ESA project ID 58351.

References

Apel, H., Thieken, A. H., Merz, B., & Blöschl, G. (2004). Flood risk assessment and associated uncertainty. *Natural Hazards and Earth System Sciences*, 4(2), 295–308. <https://doi.org/10.5194/nhess-4-295-2004>

Arns, A., Dangendorf, S., Jensen, J., Talke, S., Bender, J., & Pattiaratchi, C. (2017). Sea-level rise induced amplification of coastal protection design heights. *Scientific Reports*, 7, 40171. <https://doi.org/10.1038/srep40171>

Arns, A., Wahl, T., Wolff, C., Vafeidis, A. T., Haigh, I. D., Woodworth, P., et al. (2020). Non-linear interaction modulates global extreme sea levels, coastal flood exposure, and impacts. *Nature Communications*, 11(1), 1918. <https://doi.org/10.1038/s41467-020-15752-5>

Bates, P. D., Horritt, M., & Fewtrell, T. (2010). A simple inertial formulation of the shallow water equations for efficient two-dimensional flood inundation modelling. *Journal of Hydrology*, 387(1–2), 33–45. <https://doi.org/10.1016/j.jhydrol.2010.03.027>

Berardino, P., Fornaro, G., Lanari, R., & Sansosti, E. (2002). A new algorithm for surface deformation monitoring based on small baseline differential SAR interferograms. *IEEE Transactions on Geoscience and Remote Sensing*, 40(11), 2375–2383. <https://doi.org/10.1109/TGRS.2002.803792>

Brown, S., & Nicholls, R. J. (2015). Subsidence and human influences in mega deltas: The case of the Ganges–Brahmaputra–Meghna. *Science of the Total Environment*, 527–528, 362–374. <https://doi.org/10.1016/j.scitotenv.2015.04.124>

Curran, A., De Bruijn, K. M., & Kok, M. (2018). Influence of water level duration on dike breach triggering, focusing on system behaviour hazard analyses in lowland rivers. *Georisk: Assessment and Management of Risk for Engineered Systems and Geohazards*, 14(1), 26–40. <https://doi.org/10.1080/17499518.2018.1542498>

Dawson, R. J., Ball, T., Werritty, J., Werritty, A., Hall, J. W., & Roche, N. (2011). Assessing the effectiveness of non-structural flood management measures in the Thames Estuary under conditions of socio-economic and environmental change. *Global Environmental Change*, 21(2), 628–646. <https://doi.org/10.1016/j.gloenvcha.2011.01.013>

Dawson, R. J., Hall, J. W., Sayers, P. B., Bates, P. D., & Rosu, C. (2005). Sampling-based flood risk analysis for fluvial dike systems. *Stochastic Environmental Research and Risk Assessment*, 19(6), 388–402. <https://doi.org/10.1007/s00477-005-0010-9>

Day, J. W., Agboola, J., Chen, Z., D'Elia, C., Forbes, D. L., Giosan, L., et al. (2016). Approaches to defining deltaic sustainability in the 21st century. *Estuarine, Coastal and Shelf Science*, 183, 275–291. <https://doi.org/10.1016/j.ecss.2016.06.018>

Devlin, A. T., Jay, D. A., Zaron, E. D., Talke, S. A., Pan, J., & Lin, H. (2017). Tidal variability related to sea level variability in the Pacific Ocean. *Journal of Geophysical Research: Oceans*, 122, 8445–8463. <https://doi.org/10.1002/2017JC013165>

Dixon, T. H. (2008). Earth scientists and public policy: Have we failed New Orleans? *Eos*, 89, 96. <https://doi.org/10.1029/2008EO100005>

- Dixon, T. H., Amelung, F., Ferretti, A., Novali, F., Rocca, F., Dokka, R., et al. (2006). Space geodesy: Subsidence and flooding in New Orleans. *Nature*, *441*(7093), 587–588. <https://doi.org/10.1038/441587a>
- Douben, K. J. (2006). Characteristics of river floods and flooding: A global overview, 1985–2003. *Irrigation and Drainage*, *55*(S1), S9–S21. <https://doi.org/10.1002/ird.239>
- Du, S. Q., Scussolini, P., Ward, P. J., Zhang, M., Wen, J. H., Wang, L. Y., et al. (2020). Hard or soft flood adaptation? Advantages of a hybrid strategy for Shanghai. *Global Environmental Change*, *61*, 102037. <https://doi.org/10.1016/j.gloenvcha.2020.102037>
- Ericson, J. P., Vörösmarty, C. J., Dingman, S. L., Ward, L. G., & Meybeck, M. (2006). Effective sea-level rise and deltas: causes of change and human dimension implications. *Global and Planetary Change*, *50*(1–2), 63–82. <https://doi.org/10.1016/j.gloplacha.2005.07.004>
- EurOtop. (2016). Manual on wave overtopping of sea defences and related structures—An overtopping manual largely based on European research, but for worldwide application. In J. W. Van der Meer, N. W. H. Allsop, T. Bruce, J. De Rouck, A. Kortenhaus, T. Pullen, et al., (Eds.), www.overtopping-manual.com
- Ge, J., Ding, P., Chen, C., Hu, S., Fu, G., & Wu, L. (2013). An integrated East China Sea-Changjiang Estuary model system with aim at resolving multi-scale regional–shelf–estuarine dynamics. *Ocean Dynamics*, *63*(8), 881–900. <https://doi.org/10.1007/s10236-013-0631-3>
- Giosan, L., Syvitski, J. P. M., Constantinescu, S., & Day, J. (2014). Protect the world's deltas. *Nature*, *516*, 5–7.
- Gong, S. L., & Yang, S. L. (2008). Effect of land subsidence on urban flood prevention engineering in Shanghai. *Scientia Geographica Sinica*, *28*, 543–547. (in Chinese)
- Hall, J. W., Dawson, R. J., Sayers, P., Rosu, C., Chatterton, J., & Deakin, R. (2003). A methodology for national-scale flood risk assessment. *Journal of Water and Maritime Engineering*, *156*(3), 235–247. <https://doi.org/10.1680/wame.2003.156.3.235>
- Hallegatte, S., Green, C., Nicholls, R. J., & Corfee-Morlot, J. (2013). Future flood losses in major coastal cities. *Nature Climate Change*, *3*(9), 802–806. <https://doi.org/10.1038/nclimate1979>
- Hanson, S., Nicholls, R., Ranger, N., Hallegatte, S., Corfee-Morlot, J., Herweijer, C., & Chateau, J. (2011). A global ranking of port cities with high exposure to climate extremes. *Climatic Change*, *104*(1), 89–111. <https://doi.org/10.1007/s10584-010-9977-4>
- Hinkel, J., Lincke, D., Vafeidis, A. T., Perrette, M., Nicholls, R. J., Tol, R. S. J., et al. (2014). Coastal flood damage and adaptation costs under 21st century sea-level rise. *Proceedings of the National Academy of Sciences*, *111*(9), 3292–3297. <https://doi.org/10.1073/pnas.1222469111>
- Hoitink, A. J. F., Nittrouer, J. A., Passalacqua, P., Shaw, J. B., Langendoen, E. J., Huismans, Y., & Maren, D. S. (2020). Resilience of river deltas in the Anthropocene. *Journal of Geophysical Research*, *125*, e2019JF005201. <https://doi.org/10.1029/2019JF005201>
- IPCC. (2013). Climate Change 2013: The physical science basis. In T. F. Stocker, D. Qin, G.-K. Plattner, M. Tignor, S. K. Allen, J. Boschung, et al., (Eds.), *Contribution of Working Group I to the Fifth Assessment Report of the Intergovernmental Panel on Climate Change* (p. 1535). Cambridge, UK: Cambridge University Press.
- IPCC. (2014). Climate Change 2014: Impacts, adaptation, and vulnerability. Part A: Global and Sectoral Aspects. In C. B. Field, V. R. Barros, D. J. Dokken, K. J. Mach, M. D. Mastrandrea, T. E. Bilir, et al., (Eds.), *Contribution of Working Group II to the Fifth Assessment Report of the Intergovernmental Panel on Climate Change* (p. 1132). Cambridge, UK: Cambridge University Press.
- Jongman, B. (2018). Effective adaptation to rising flood risk. *Nature Communications*, *9*, 1986. <https://doi.org/10.1038/s41467-018-04396-1>
- Jongman, B., Ward, P. J., & Aerts, J. C. (2012). Global exposure to river and coastal flooding: Long term trends and changes. *Global Environmental Change*, *22*(4), 823–835. <https://doi.org/10.1016/j.gloenvcha.2012.07.004>
- Jonkman, S. N. (2013). Advanced flood risk analysis required. *Nature Climate Change*, *3*, 1004. <https://doi.org/10.1038/nclimate2031>
- Kates, R. W., Colten, C. E., Laska, S., & Leatherman, S. P. (2006). Reconstruction of New Orleans after Hurricane Katrina: A research perspective. *Proceedings of the National Academy of Sciences*, *103*(40), 14,653–14,660. <https://doi.org/10.1073/pnas.0605726103>
- Kopp, R. E., Horton, R. M., Little, C. M., Mitrovica, J. X., Oppenheimer, M., Rasmussen, D. J., et al. (2014). Probabilistic 21st and 22nd century sea level projections at a global network of tide gauge sites. *Earth's Future*, *2*, 383–406. <https://doi.org/10.1002/2014EF000239>
- Lanari, R., Casu, F., Manzo, M., Zeni, G., Berardino, P., & Manunta, M. (2007). An overview of the small baseline subset algorithm: A DInSAR technique for surface deformation analysis. *Pure and Applied Geophysics*, *164*(4), 637–661. <https://doi.org/10.1007/s00024-007-0192-9>
- Li, L., Switzer, A. D., Wang, Y., Chan, C., Qiu, Q., & Weiss, R. (2018). A modest 0.5-m rise in sea level will double the tsunami hazard in Macau. *Science Advances*, *4*, eaat1180. <https://doi.org/10.1126/sciadv.aat1180>
- Lin, N., & Emanuel, K. (2016). Grey swan tropical cyclones. *Nature Climate Change*, *6*(1), 106–111. <https://doi.org/10.1038/nclimate2777>
- Lin, N., Emanuel, K., Oppenheimer, M., & Vanmarcke, E. (2012). Physically based assessment of hurricane surge threat under climate change. *Nature Climate Change*, *2*(6), 462–467. <https://doi.org/10.1038/nclimate1389>
- Menéndez, M., & Woodworth, P. L. (2010). Changes in extreme high water levels based on a quasi-global tide-gauge data set. *Journal of Geophysical Research*, *115*, C10011. <https://doi.org/10.1029/2009JC005997>
- Miller, K. G., Kopp, R. E., Horton, B. P., Browning, J. V., & Kemp, A. C. (2013). A geological perspective on sea-level rise and impacts along the U.S. mid-Atlantic coast. *Earth's Future*, *1*, 3–18. <https://doi.org/10.1002/2013EF000135>
- Minderhoud, P. S. J., Coumou, L., Erkens, G., Middelkoop, H., & Stouthamer, E. (2019). Mekong delta much lower than previously assumed in sea-level rise impact assessments. *Nature Communications*, *10*, 3847. <https://doi.org/10.1038/s41467-019-11602-1>
- Moftakhari, H. R., Salvadori, G., AghaKouchak, A., Sanders, B. F., & Matthew, R. A. (2017). Compounding effects of sea level rise and fluvial flooding. *Proceedings of the National Academy of Sciences*, *114*(37), 9785–9790. <https://doi.org/10.1073/pnas.1620325114>
- Naulin, M., Kortenhaus, A., & Oumeraci, H. (2015). Reliability-based flood defense analysis in an integrated risk assessment. *Coastal Engineering Journal*, *57*, 1540005. <https://doi.org/10.1142/S0578563415400057>
- Nienhuis, J. H., Ashton, A. D., Edmonds, D. A., Hoitink, A. J. F., Kettner, A. J., Rowland, J. C., & Törnqvist, T. E. (2020). Global-scale human impact on delta morphology has led to net land area gain. *Nature*, *577*(7791), 514–518. <https://doi.org/10.1038/s41586-019-1905-9>
- Nienhuis, J. H., Hoitink, A. J. F. T., & Törnqvist, T. E. (2018). Future change to tide-influenced deltas. *Geophysical Research Letters*, *45*, 3499–3507. <https://doi.org/10.1029/2018GL077638>
- Pepe, A., Bonano, M., Zhao, Q., Yang, T., & Wang, H. (2016). The use of C-/X-band time-gapped SAR data and geotechnical models for the study of Shanghai's ocean-reclaimed lands through the SBAS-DInSAR technique. *Remote Sensing*, *8*, 911. <https://doi.org/10.3390/rs8110911>
- Ruig, L. T., Barnard, P. L., Botzen, W., Grifman, P., Hart, J. F., Moel, H., et al. (2019). An economic evaluation of adaptation pathways in coastal mega cities: An illustration for Los Angeles. *Science of the Total Environment*, *678*, 647–659. <https://doi.org/10.1016/j.scitotenv.2019.04.308>
- Schubert, J. E., & Sanders, B. F. (2012). Building treatments for urban flood inundation models and implications for predictive skill and modeling efficiency. *Advances in Water Resources*, *41*, 49–64. <https://doi.org/10.1016/j.advwatres.2012.02.012>

- Shirzaei, M., & Bürgmann, R. (2018). Global climate change and local land subsidence exacerbate inundation risk to the San Francisco Bay Area. *Science Advances*, 4, eaap9234. <https://doi.org/10.1126/sciadv.aap9234>
- State Oceanic Administration People's Republic of China (2016). China sea level bulletin 2015. (in Chinese).
- Syvitski, J. P. M., Kettner, A. J., Overeem, I., Hutton, E. W. H., Hannon, M. T., & Brakenridge, G. R. (2009). Sinking deltas due to human activities. *Nature Geoscience*, 2(10), 681–686. <https://doi.org/10.1038/ngeo0629>
- Tessler, Z. D., Vörösmarty, C. J., Grossberg, M., Gladkova, I., Aizenman, H., Syvitski, J. P. M., & Fofoula-Georgiou, E. (2015). Profiling risk and sustainability in coastal deltas of the world. *Science*, 349(6248), 638–643. <https://doi.org/10.1126/science.aab3574>
- Törnqvist, T. E., Wallace, D. J., Storms, J. E. A., Wallinga, J., van Dam, R. L., Blauuw, M., et al. (2008). Mississippi Delta subsidence primarily caused by compaction of Holocene strata. *Nature Geoscience*, 1(3), 173–176. <https://doi.org/10.1038/ngeo129>
- Vorogushyn, S., Merz, B., & Apel, H. (2009). Development of dike fragility curves for piping and micro-instability breach mechanisms. *Natural Hazards and Earth System Sciences*, 9(4), 1383–1401. <https://doi.org/10.5194/nhess-9-1383-2009>
- Vorogushyn, S., Merz, B., Lindenschmidt, K. E., & Apel, H. (2010). A new methodology for flood hazard assessment considering dike breaches. *Water Resources Research*, 46, W08541. <https://doi.org/10.1029/2009WR008475>
- Wahl, T. (2017). Sea-level rise and storm surges, relationship status: complicated! *Environmental Research Letters*, 12, 111001. <https://doi.org/10.1088/1748-9326/aa8eba>
- Wang, J., Gao, W., Xu, S. Y., & Yu, L. Z. (2012). Evaluation of the combined risk of sea level rise, land subsidence, and storm surges on the coastal areas of Shanghai, China. *Climatic Change*, 115(3–4), 537–558. <https://doi.org/10.1007/s10584-012-0468-7>
- Wang, J., Yi, S., Li, M. Y., Wang, L., & Song, C. C. (2018). Effects of sea level rise, land subsidence, bathymetric change and typhoon tracks on storm flooding in the coastal areas of Shanghai. *Science of the Total Environment*, 621, 228–234. <https://doi.org/10.1016/j.scitotenv.2017.11.224>
- Wang, Z. Q. (2016). Reliability analysis for the flood defence system along the Huangpu River, Shanghai. Master Thesis, Delft University of Technology, the Netherlands.
- Ward, P. J., Couasnon, A., Eilander, D., Haigh, I. D., Hendry, A., Muis, S., et al. (2018). Dependence between high sea-level and high river discharge increases flood hazard in global deltas and estuaries. *Environmental Research Letters*, 13, 084012. <https://doi.org/10.1088/1748-9326/aad400>
- Ward, P. J., Jongman, B., Aerts, J. C., Bates, P. D., Botzen, W., Loaiza, A. D., et al. (2017). A global framework for future costs and benefits of river flood protection in urban areas. *Nature Climate Change*, 7(9), 642–646. <https://doi.org/10.1038/nclimate3350>
- Winsemius, H. C., Aerts, J. C., Beek, L., Bierkens, M., Bouwman, A., Jongman, B., et al. (2016). Global drivers of future river flood risk. *Nature Climate Change*, 6(4), 381–385. <https://doi.org/10.1038/nclimate2893>
- Woodruff, J. D., Irish, J. L., & Camargo, S. J. (2013). Coastal flooding by tropical cyclones and sea-level rise. *Nature*, 504(7478), 44–52. <https://doi.org/10.1038/nature12855>
- Xian, S. Y., Yin, J., Lin, N., & Oppenheimer, M. (2018). Influence of risk factors and past events on flood resilience in coastal megacities: Comparative analysis of NYC and Shanghai. *Science of the Total Environment*, 610–611, 1251–1261. <https://doi.org/10.1016/j.scitotenv.2017.07.229>
- Yang, P., Tang, Y. Q., Zhou, N. Q., & Wang, J. X. (2008). Consolidation settlement of Shanghai dredger fill under self-weight using centrifuge modeling test. *Journal of Central South University of Technology*, 39, 862–866. (in Chinese)
- Yin, J., Lin, N., & Yu, D. (2016). Coupled modeling of storm surge and coastal inundation: a case study in New York City during Hurricane Sandy. *Water Resources Research*, 52, 8685–8699. <https://doi.org/10.1002/2016WR019102>
- Yin, J., Yu, D., Yin, Z., Wang, J., & Xu, S. (2013). Modelling the combined impacts of sea-level rise and land subsidence on storm tides induced flooding of the Huangpu River in Shanghai, China. *Climatic Change*, 119(3–4), 919–932. <https://doi.org/10.1007/s10584-013-0749-9>
- Yin, J., Yu, D., Yin, Z., Wang, J., & Xu, S. (2015). Modelling the anthropogenic impacts on fluvial flood risks in a coastal mega-city: a scenario-based case study in Shanghai, China. *Landscape and Urban Planning*, 136, 144–155. <https://doi.org/10.1016/j.landurbplan.2014.12.009>
- Yin, J., Zhao, Q., Yu, D., Lin, N., Kubanek, K., Ma, G., et al. (2019). Long-term flood-hazard modeling for coastal areas using InSAR measurements and a hydrodynamic model: The case study of Lingang New City, Shanghai. *Journal of Hydrology*, 571, 593–604. <https://doi.org/10.1016/j.jhydrol.2019.02.015>
- Yu, D., & Lane, S. N. (2006). Urban fluvial flood modelling using a two-dimensional diffusion wave treatment, part 1: mesh resolution effects. *Hydrological Processes*, 20(7), 1541–1565. <https://doi.org/10.1002/hyp.5935>
- Yu, D., & Lane, S. N. (2011). Interaction between subgrid-scale resolution, feature representation and grid-scale resolution in flood inundation modelling. *Hydrological Processes*, 25(1), 36–53. <https://doi.org/10.1002/hyp.7813>
- Zhang, K., Douglas, B. C., & Leatherman, S. P. (2000). Twentieth-century storm activity along the US east coast. *Journal of Climate*, 13(10), 1748–1761. [https://doi.org/10.1175/1520-0442\(2000\)013<1748:TCSAAT>2.0.CO;2](https://doi.org/10.1175/1520-0442(2000)013<1748:TCSAAT>2.0.CO;2)
- Zhang, W., Villarini, G., Vecchi, G. A., & Smith, J. A. (2018). Urbanization exacerbated the rainfall and flooding caused by hurricane Harvey in Houston. *Nature*, 563(7731), 384–388. <https://doi.org/10.1038/s41586-018-0676-z>
- Zhang, Y., Chen, G., Hu, J., Chen, X., Yang, W., Tao, A., & Zheng, J. (2017). Experimental study on mechanism of sea-dike failure due to wave overtopping. *Applied Ocean Research*, 68, 171–181. <https://doi.org/10.1016/j.apor.2017.08.009>
- Zhao, Q., Pepe, A., Gao, W., Lu, Z., Bonano, M., He, M., et al. (2015). A DInSAR investigation of the ground settlement time evolution of ocean-reclaimed lands in Shanghai. *IEEE Journal of Selected Topics in Applied Earth Observations and Remote Sensing*, 8(4), 1763–1781. <https://doi.org/10.1109/JSTARS.2015.2402168>